HHS Public Access

Author manuscript

Arterioscler Thromb Vasc Biol. Author manuscript; available in PMC 2019 September 01.

Published in final edited form as:

Arterioscler Thromb Vasc Biol. 2018 September ; 38(9): 2065–2078. doi:10.1161/ATVBAHA.118.311290.

INTERACTION BETWEEN PANNEXIN 1 AND CAVEOLIN-1 IN SMOOTH MUSCLE CAN REGULATE BLOOD PRESSURE

Leon J. DeLalio[1,2], **Alexander S. Keller**[1,2], **Jiwang Chen**[3], **Andrew K.J. Boyce**[4], **Mykhaylo Artamonov**[5], **Henry R. Askew-Page**[1], **T.C. Stevenson Keller IV**[1,5], **Scott R. Johnstone**[1], **Rachel B. Weaver**[1], **Miranda E. Good**[1], **Sara Murphy**[1], **Angela K. Best**[1], **Ellen L. Mintz**[6], **Silvia Penuela**[7], **Iain Greenwood**[9], **Roberto F. Machado**[10], **Avril V. Somlyo**[5], **Leigh Anne Swayne**[4], **Richard Minshall**[9], and **Brant E. Isakson**[1,5,*]

[1]Robert M. Berne Cardiovascular Research Center, University of Virginia School of Medicine, Charlottesville, VA

[2]Department of Pharmacology, University of Virginia School of Medicine, Charlottesville, VA

[3]Department of Medicine, The University of Illinois at Chicago, Chicago, IL

[4]Division of Medical Sciences, Centre for Biomedical Research, University of Victoria, Victoria, BC Canada

[5]Department of Molecular Physiology and Biophysics, University of Virginia, Charlottesville, VA

[6]Department of Biomedical Engineering, University of Virginia School of Engineering, Charlottesville, VA

[7]Department of Anatomy and Cell Biology, Schulich Scholl of Medicine and Dentistry, University of Western Ontario, London ON, Canada

[9]Molecular and Clinical Sciences Research Institute, St. George's University London UK

[9]Department of Pharmacology and Department of Anesthesiology, The University of Illinois at Chicago, Chicago, IL

[10]Division of Pulmonary, Critical Care, Sleep, & Occupational Medicine, Indiana University School of Medicine, Indianapolis, IN

Abstract

Objective—Sympathetic nerve innervation of vascular smooth muscle cells (VSMCs) is a major regulator of arteriolar vasoconstriction, vascular resistance, and blood pressure (BP). Importantly, α-adrenergic receptor stimulation, which uniquely couples with Pannexin 1 (Panx1) channel-mediated ATP release channels in resistance arteries, also requires localization to membrane caveolae. Here we test if localization of Panx1 to caveolin-1 promotes channel function (stimulus-dependent ATP release and adrenergic vasoconstriction) and is important for BP homeostasis.

*Corresponding Author: Brant E. Isakson, University of Virginia School of Medicine, 409 Lane Rd, MR4 Building; Rm 6071, Charlottesville, VA, 22901 E: brant@virginia.edu, P:434-924-2093, F: 434-924-2828.

DISCLOSURES: The authors have no conflicts to disclose.

Approach and Results—We use *in vitro* VSMC culture models, *ex vivo* resistance arteries, and a novel inducible VSMC-specific caveolin-1 knockout mouse to probe interactions between Panx1 and caveolin-1. We report that Panx1 and caveolin-1 co-localized on the VSMC plasma membrane of resistance arteries near sympathetic nerves in an adrenergic stimulus-dependent manner. Genetic deletion of caveolin-1 significantly blunts adrenergic stimulated ATP release and vasoconstriction, with no direct influence on endothelium-dependent vasodilation or cardiac function. A significant reduction in mean arterial pressure (Total= 4 mmHg; Night= 7 mmHg) occurred in mice deficient for VSMC caveolin-1. These animals were resistant to further BP lowering using a Panx1 peptide inhibitor PxIL2P1, which targets an intracellular loop region necessary for channel function.

Conclusions—Translocalization of Panx1 to caveolin-1-enriched caveolae in VSMCs augments the release of purinergic stimuli necessary for proper adrenergic-mediated vasoconstriction and BP homeostasis.

Keywords

Pannexin 1; caveolin-1; caveolae; blood pressure; α-adrenergic receptor; smooth muscle

INTRODUCTION

In the peripheral circulatory system, blood pressure (BP) homeostasis is largely regulated by the contractile state of the smooth muscle cells (VSMCs) in the wall of resistance arteries. Resistance arteries are small diameter (≤200 μm) arterioles that are composed of an intimal endothelial layer, a tunica media consisting of one to two VSMC layers[1], and are functionally defined by the ability to respond to changes in intraluminal pressure to control vascular resistance and blood flow. Sympathetic nerve innervation of VSMCs is a major regulatory pathway that induces VSMC constriction, thus altering arteriolar lumen diameter and increasing the amount of vascular resistance[2,3]. While much is already known about the induction of rapid (purinergic) and potentiated (adrenergic) sympathetic nerve-derived stimuli on function of resistance arteries[4], less is known about the identity of downstream VSMC signaling molecules that subsequently coordinate VSMC-derived stimuli in the arteriolar wall. Signaling through α-adrenergic receptors (α-ARs) and activation of plasma membrane-associated signaling molecules may be compartmentalized by caveolae near areas of sympathetic innervation[2,5–8].

Caveolae are specialized plasma membrane domains that play an important role in intracellular signaling, cellular transport, and differentiation[9–11]. Caveolae are defined by their hallmark plasma membrane morphology, consisting of 80–100nm-wide membrane invaginations, and by their composition of oligomeric coat-forming proteins called caveolins[12]. Of the three caveolin isoforms, caveolin-1 is essential for caveolae formation and function[13–15]. Caveolin-1 has been shown to regulate vasoconstriction responses in small arterioles and to influence BP homeostasis in animal models[13,16–18]. Importantly, caveolin-1 is expressed in VSMCs of small arteries and acts as a membrane-scaffold protein for both α-ARs and downstream G-protein dependent vasoconstriction signaling molecules[19,20], suggestive of a role in adrenergic-mediated vasoconstriction.

Recently, our group and others[21–24] have elucidated in mouse and humans an α–AR signaling axis that activates Pannexin 1 channels. Pannexins are a family of transmembrane channel-forming glycoproteins that have emerged as the physiological conduit for controlled ATP release from vascular and non-vascular cell types[25–27]. We have previously reported that Panx1 expression is polarized within the vascular tree, with high expression levels in VSMCs of resistance arteries (e.g. mesenteric, cremasteric, thoracodorsal, and coronary), but is not present in large conduit vessels such as the femoral and carotid arteries, and the aorta[28]. This expression pattern suggests a unique role for Panx1 in regulating vascular resistance. Using Panx1 pharmacological inhibitors and inducible VSMC-specific Panx1 knockout mice, we have further demonstrated that Panx1-mediated ATP release and vasoconstriction are uniquely coupled with α-adrenergic stimulation and are crucial for maintaining BP homeostasis[21,22]. Multiple groups have confirmed the activation of Panx1 channels by α-adrenergic stimulation[29–31], thus demonstrating ATP release through Panx1 as a significant physiological pathway for integrating and coordinating VSMC-derived constriction responses[4,32].

In the present study, we hypothesized that caveolin-1 acts as a molecular scaffold that concentrates VSMC Panx1 to areas important for sympathetic nerve innervation, thus supporting α-adrenergic vasoconstriction and BP homeostasis. In response to the α-adrenergic agonist phenylephrine we observed a novel interaction and co-localization of caveolin-1 and Panx1 to regions of innervation at the VSMC plasma membrane. To investigate the functional role of caveolin-1 during α-adrenergic mediated responses, we generated an inducible, VSMC-specific caveolin-1 knockout mouse model. We show that VSMC-derived caveolin-1 is required for α-adrenergic stimulated ATP release and adrenergic vasoconstriction. Deletion of VSMC caveolin-1 results in a significant reduction in mean arterial BP, particularly during the nocturnal (active) period when sympathetic drive is high. Furthermore, we suggest that caveolin-1 mediated BP effects are regulated through the Panx1 intracellular loop regulatory domain, previously identified to be indispensable for α-adrenergic vasoconstriction[22].

METHODS

Data and Materials

All data will be made available upon request by the corresponding authors at the University of Virginia.

Animals

All animals were cared for under the provisions of the University of Virginia Animal Care and Use Committee and the National Institute of Health guidelines for the care and use of laboratory animals. Male C57BL/6 mice between 10–15 weeks of age were purchased from Taconic. Male smooth muscle myosin heavy chain-Cre recombinase modified estrogen receptor binding domain (SMMHC-CreER^{T2}) modified mice, a kind gift from S. Offermanns[33], were used for experimentation due to the restrictive presence of Cre recombinase on the Y chromosome. Aortae from Connexin 43 globally deficient mice (Cx43$^{-/-}$) were harvested at birth. Mice harboring lox-P recombination sites for caveolin-1

(Caveolin-$1^{fl/fl}$) were generated as previously described[34]. SMMHC-$CreER^{T2}$ mice were mated with Caveolin-$1^{fl/fl}$ mice to specifically delete caveolin-1 from vascular smooth muscle cells. Induction of Cre-mediated deletion was performed at 6 weeks of age via ten daily intraperitoneal injections (100 μl) of tamoxifen (1 mg/kg) to generate caveolin-1 null animals (SMMHC-$CreER^{T2+}$/$Cav1^{\Delta/\Delta}$) or ten daily 100 μl injections of peanut oil (vehicle control) to generate control animals (SMMHC-$CreER^{T2+}$/$Cav1^{fl/fl}$). All animal experiments were performed at the least 14-days from the final injection with tamoxifen and/or peanut oil since the Cre recombinase is located on the Y. Mice lacking the Cre recombinase allele were also used as tamoxifen controls. Please see the Major Resources Table in Supplemental Material for detail.

Cell Culture

Primary human vascular coronary smooth muscle cells (VSMCs) were purchased from Lonza (Cat# CC-2583). All cells were maintained under standard cell culture conditions (5% CO_2 at 37°C) in smooth muscle growth media (Lonza; Cat# CC-3181) supplemented with smooth muscle growth factors (Lonza; Cat# CC-3182) and 10% fetal bovine serum (FBS) (Lonza; Cat# CC-4102D). Cells were used at 8 passages or fewer for *in vitro* experiments. For all experiments, VSMCs were serum deprived for 48hrs in 0.2% FBS to induce contractile phenotypes[35–37].

Ultrastructure electron microscopy

Mouse arteries were processed for ultrastructure TEM as previously described[38]. Images were obtained using a Joel 1230 transmission electron microscope at the Advanced Microscopy Core at the University of Virginia.

Proximity Ligation Assay (PLA) and Immunofluorescence

Thoracodorsal arteries (TDA) were isolated as previously described[39], incubated in Krebs-HEPES physiological saline buffer, and treated with phenylephrine (20 μmol/L) in a single well of a 96-well dish. TDAs were then placed in a 1.5 mL Eppendorf tube, fixed in 4% paraformaldehyde, and subjected to *en face* proximity ligation assay using the Duolink *in situ* PLA detection kit (Sigma) as previously described by us[40]. Sympathetic nerves were labeled using anti-mouse tyrosine hydroxylase antibody (Abcam #ab112; 1:250 dilution) and visualized using an Alexa Fluor 568 secondary antibody (Life Technologies #A-21099; 1:400 dilution). Primary antibodies for PLA labeling included anti-mouse Caveolin-1 (BD Biosciences# 610406, clone 2297; 1:400 dilution) and anti-mouse Panx1 CT395 (characterized by Penuela et al,[41] 1:300 dilution). PLA detection was performed according to manufacturer's protocol. Immunofluorescence staining on aorta and TDAs was performed as previously described[28]. Primary antibodies for immunofluorescence included anti-rabbit Cx43 antibody (Sigma #C6219; 1:300 dilution) and vesicular nucleotide transport protein (anti-mouse VNUT; a kind gift from Dr. Chen Li, 1:200 dilution). All images were acquired using an Olympus Fluoview 1000 confocal microscope. PLA punctate spots were counted per $100um^2$ cell area. Caveolin-1 deletion was quantified using batch-processed tissue and threshold generated images. The relative fluorescence intensity within the smooth muscle cell layer (demarcated by co-association with Acta2 staining, and between the boundary lines of the IEL and adipose tissue) was measured using ImageJ[42] and normalized to Acta2

positive area. Co-staining for smooth muscle cells (Acta2; Sigma #A2547, 1:500 dilution) and endothelial cells (PECAM-1; Santa Cruz #sc28188, 1:400 dilution) was performed. Data are presented as mean ± SEM. A students t-test was performed for statistical significance. *p < 0.05.

Live cell imaging

Confocal imaging was performed with a Leica TCS SP8 confocal microscope. Human VSMCs were cultured as indicated above and plated on 100μg/mL poly-D-lysine (PDL) on cover glass. Cells were transfected with plasmids encoding Panx1-RFP[43] and Caveolin-1-GFP using jetPRIME (Polyplus transfection/VWR) according to the manufacturer's protocol. Image acquisition and co-distribution analyses were performed double-blinded to treatment conditions with identical imaging parameters. For live imaging, baseline images were collected at 30 sec intervals for 2 min using a 20X (0.7 NA) objective. Importantly, the large cellular size (range of lengths) permitted imaging of only one cell per field of view. Treatment with phenylephrine (100 μmol/L; Sigma-Aldrich), ATP (500μmol/L; Sigma–Aldrich) or vehicle control (water) was performed by removing half the volume of control media and replacing it with the same volume of media containing 2X agonist. Images were collected at 30 sec intervals up to 5 min. The z-section containing the largest cellular area was selected for Mander's coefficient analysis of Panx1-Cav1 co-distribution using the JACoP plugin in FIJI[44]. All post-treatment data were normalized to the average obtained at baseline. Data were collected from N=5–11 cells per experimental condition and analyzed using a two-way ANOVA for time and treatment (Time: $F(10, 250) = 3.027$, $P = 0.0012$; Treatment: $F(2, 25) = 4.673$, $P = 0.0189$; Subjects: $F(25, 250) = 19.41$, $P < 0.0001$) with Dunnett's posthoc ($P<0.05$ for phenylephrine at 0.5 min, for ATP) with GraphPad Prism v5.0.

Membrane fractionation and isolation of caveolin-1 enriched membrane domains

Human VSMCs were grown to confluence and incubated in media containing 0.2% FBS for 48 hr prior to use. VSMCs were washed with PBS and re-equilibrated for 10 min in Krebs buffer (mmol/L: 118.4 NaCl, 4.7 KCl, 1.2 $MgSO_4$, 4 $NaHCO_3$, 1.2 KH_2PO_4, 10 Hepes, 6 Glucose) containing 2 mmol/L $CaCl_2$. VSMCs were treated with 100μmol/L phenylephrine or vehicle control, scraped with a cell scraper and lysed in ice-cold detergent-free lysis buffer (500 mmol/L Na_2CO_3, 50 mmol/L NaF, 2 mmol/L Na_3VO_4, pH 11, supplemented with 1 mg/mL of protease inhibitor cocktail (Sigma) and 1 mg/mL P2 and P3 phosphatase inhibitor cocktails (Sigma)). Lysates were homogenized using a dounce homogenizer (10 strokes) and sonication (25 pulses for 1 sec) on ice. Lysates were either fractioned using differential centrifugation (40,000 rpm; 1hr Beckman XL80 ultracentrifuge with Sw55Ti rotor) or using centrifugation across a sucrose gradient. To create a sucrose gradient, sucrose solutions were mixed in MBS-sodium carbonate buffer (25 mmol/L MES, 0.5 M NaCl, 250 mmol/L Na_2CO_3) to 85%, 30%, and 5% by mass by adding 42.5 g, 15 g, or 2.5 g of sucrose, respectively, to 50 mL of MBS. Lysates were mixed with equal volume of 85% sucrose solution to create 42.5% layer. 1.5 mL of 42.5% layer was added to the bottom of a Sw55Ti ultracentrifuge tube, after which a 5–42.5% discontinuous sucrose gradient was formed by adding, dropwise on top of previous layers, 1 mL of 30% sucrose solution followed by 1 mL of 5% sucrose solution. Gradients were centrifuged at 42,000 rpm for 18 hr in a Beckman

XL80 ultracentrifuge with Sw55Ti rotor. Ten fractions of 350 μL each were removed starting from the top of the gradient and analyzed using western blot with antibodies for rabbit anti-human Pannexin 1 (characterized by Penuela et al.[45] 1:1000 dilution) and mouse anti-caveolin-1 (BD Biosciences #610406; 1:1000 dilution). Co-immunoprecipitation was performed using either Pannexin1 antibodies (1:50 dilution) in conjunction with anti-rabbit IgG Dynabeads (Invitrogen) respectively. To perform co-immunoprecipitations, caveolin-1-enriched fractions (4–5) and non-enriched fractions (7–8) were combined and total protein from each was measured by BCA assay. Equal amounts of protein from each pair of fractions was used for co-immunoprecipitation as described above. Five independent experiments were performed. The ratio of caveolin-1 signal was normalized to the amount of immunoprecipitated Pannexin 1. Data are represented as mean ±SEM. A students t-test was performed for statistical significance. *$p < 0.05$.

Western blot

After stimulation with adrenergic agonists, human VSMCs were homogenized in ice-cold NP-40 extraction buffer (50mmol/L Tris-HCL, 150mmol/L NaCl, 5mmol/L EDTA, 1% deoxycholate, 1% NP-40 and 1% Triton-X100 in PBS and pH adjusted to 7.4) containing protease inhibitor cocktail (Sigma) and P2 / P3 phosphatase inhibitor cocktail (Sigma). Cell/tissue lysates were incubated at 4°C for 10 min to solubilize proteins, sonicated for 12 pulses for 1 sec each, and centrifuged for 10 min at 12,000 rpm to pellet cell debris. Protein concentration was determined using the BCA method (Pierce). 10–20 μg of total protein was loaded into each sample well. Samples were subjected to SDS gel electrophoresis using 4–12% Bis-Tris gels (Invitrogen) and transferred to nitrocellulose membrane for immunoblotting. Membranes were blocked for 1 hour at room temperature in a solution containing 3% BSA in Tris buffered saline, then incubated overnight at 4°C with primary antibodies against rabbit anti-Pannexin 1 (Cell Signaling Technology #91137 (D9M1C); 1:1000 dilution), rabbit anti-Caveolin-1 (BD Biosciences #610059; 1:1000 dilution), rabbit anti-transferrin receptor (Abcam #ab84036; 1:1000 dilution) and mouse anti-GAPDH (Sigma mAb #G8795; 1:10,000). Membranes were washed and incubated in LiCOR IR Dye secondary antibodies (1:15,000) for 1 hour and viewed/quantified using the LiCOR Odyssey with Image Studio software. Representative western blot images have been cropped for presentation.

Pressure myography

Pressure myography was performed on TDAs as previously described[46]. Briefly, mice were sacrificed using CO_2 asphyxia. TDAs were microdissected, cannulated on glass pipettes in a temperature-controlled pressure arteriography chamber, and pressurized to 80mmHg. After a 30-min equilibration period in Krebs-HEPES with 2mmol/L Ca^{2+}, vessels were treated with cumulative doses of phenylephrine (PE, 10^{-10}–10^{-3} mol/L) applied to the bath. The luminal diameter was analyzed using digital calipers in the DMT vessel acquisition software (Danish Myo Technology). Smooth muscle cell viability was assessed using serotonin (1 μmol/L) and KCl (30 mmol/L). Endothelial-dependent vasodilation was measured using cumulative doses of acetylcholine (10^{-11}–10^{-2} mol/L) as previously described[46]. A two-way analysis of variance (ANOVA) with Bonferonni post-hoc test was performed for multiple comparisons.

Concentration-effect curves were fitted to the data using four-parameter, non-linear regression curve fitting using GraphPad (version 7).

ATP measurements

For the measurement of extracellular ATP, intact TDAs of equal length were placed in individual wells of a 96-well plate in Krebs-Hepes physiologic solution for 15 min. The ectonucleotidase inhibitor ARL 67156 trisodium (Tocris; 100μmol/L) was added 30 min prior to treatment with contractile agonists as previously described[22]. Vasoconstrictor compounds were added to the incubation media for 5 min to allow ATP accumulation: Phenylephrine (PE; 20μmol/L), Norepinephrine (NE; 20 μmol/L), Serotonin (5-HT; 40nmol/L), and Endothelin-1 (ET-1; 40nmol/L) (all purchased from Sigma). Following stimulation, the media surrounding the vessel was collected and immediately placed into pre-chilled 1.5 mL Eppendorf tubes on ice. All samples were centrifuged at 10,000 x *g* for 5 min. For intracellular ATP measurements, TDAs were microdissected, cleaned of adventitia, and cut into equal 10.5mm vessel segments. Segments were individually lysed in ATP lysis buffer according to manufacturer's protocol, spun at 10,000 x g for 1 min, and samples collected. ATP concentration in the incubation media was quantified using the ATP bioluminescence assay kit HSII (Roche) using a FluoStar Omega plate reader luminometer. Extracellular ATP measurements for each sample were tested in triplicate and calculated using an ATP standard curve for all experiments. Intracellular ATP measurements were measured from three vessel segments (one TDA in triplicate). Data are presented as % change in ATP release from baseline (unstimulated) or as the concentration of ATP in the media compared to control samples. One-way ANOVA with Tukey's test was performed for statistical significance of extracellular ATP. A Kruskal-Wallis (one-way ANOVA on ranks) with Dunn's post-hoc test performed for intracellular ATP. Significance denoted as *$p < 0.05$.

Blood pressure telemetry

Blood pressure was measured using telemetry equipment as previously described[22]. Briefly, telemeters (Data Sciences International [DSI]) were implanted in C57BL/6 or SMMHC-CreER^{T2+}/Cav1$^{fl/fl}$ (SMC-Cav1$^{fl/fl}$) mice. Under isoflurane anesthesia, the catheter of a single telemetry unit (TA11PA-C10, DSI) was implanted in the left carotid artery and the transmitter placed in a subcutaneous pouch along the right flank of the mouse. After implantation surgery, mice were allowed to recover for 7 days to re-establish normal circadian rhythms and blood pressure. For experiments using inducible Cre recombinase, mouse blood pressure baselines were continuously recorded using Dataquest A.R.T. 20 software (DSI) for 5 days after normal recovery and before starting intraperitoneal tamoxifen injections or vehicle control (peanut oil) for 10 days. Blood pressure was recorded for an additional 5 days starting 24 hr after the last tamoxifen injection. Change in MAP (ΔMAP) was calculated by subtracting the average MAP measured before tamoxifen injections to the MAP after tamoxifen injections. Diurnal (inactive period) MAP was measured during animal's light cycle: 6:00 a.m. to 5:59 p.m., and nocturnal (active period) MAP was measured during the animal's dark cycle: 6:00 p.m. to 5:59 a.m. MAPs before and after tamoxifen injections were compared with a Wilcoxon test (nonparametric paired t-test). C57BL/6 mice similarly received intraperitoneal injections of tamoxifen or vehicle control,

and basal blood pressure was measured as for transgenic animals. For assessment of the blood pressure effects of the PxIL2P peptide inhibitor (formerly referred to as PxIL2P1 peptide[22]), animals were intraperitoneally injected with saline vehicle control or peptide (20 mg/kg in a volume not exceeding 100 μL). Blood pressure was recorded for 2 hr after injection, and the MAP data was averaged and compared to the basal blood pressure. Change in MAP (ΔMAP) was calculated by subtracting the baseline MAP 30 min before injection from the MAP measured during the final 30 min of the 2 hr treatment period. Data represent mean ±SEM. Two-way ANOVA with Tukey post-hoc test was performed for assessment of MAP before and after tamoxifen/vehicle control induction and for mice treated with scrambled peptide or PxIL2P peptide inhibitor.

Cardiac magnetic resonance imaging and histology

All MRI animal studies were performed under protocols that comply with the Guide for the Care and Use of Laboratory Animals (NIH publication no. 85-23, Revised 1996) and were approved by the Animal Care and Use Committee at our institution (ACUC, UVA). Mice were positioned supine in the scanner and body temperature was maintained at 36 ± 0.5°C using thermostatic circulating water. Anesthesia used was 1.25% isoflurane in O_2 inhaled through a nose cone during imaging. A 30 mm-diameter cylindrical birdcage RF coil (Bruker) with an active length of 70 mm was used, and heart rate, respiration, and temperature were monitored during imaging using a fiber optic, MR-compatible system (Small Animal Imaging Inc., Stony Brook, NY). MRI was performed on a 7 Tesla (T) Clinscan system (Bruker, Ettlingen, Germany) equipped with actively shielded gradients with a full strength of 650 mT/m and a slew rate of 6666 mT/m/ms. Baseline LV structure and function were assessed[47]. Six short-axis slices were acquired from base to apex, with slice thickness equal to 1mm, in-plane spatial resolution of 0.2 × 0.2 mm^2, and temporal resolution of 8–12 ms. Baseline ejection fraction (EF), end-diastolic volume (EDV), end-systolic volume (ESV), myocardial mass, wall thickness, and wall thickening were measured from the cine images using the freely available software Segment version 2.0 R5292 (http://segment.heiberg.se). EDV and ESV were then indexed to body mass (EDVI and ESVI, respectively). Mass to volume ratio (MVR) was calculated as the ratio of myocardial mass to EDV.

Plasma Renin ELISA

Mice were anesthetized using 2,2-Dicholor-1,1-difluoroethyl methyl ether (ThermoFisher; #76-38-0). 100–150 μl of whole blood was collected from mouse tail veins using heparinized capillary tubes into 1.5mL Eppendorf, stored on ice, and centrifuged for 15 minutes at 1000rpm. Plasma was aliquoted, snap frozen, and stored at −80°C. Plasma renin concentration was measured using a total renin ELISA (RayBio; #ELM-Ren1) against a renin standard curve with 1:15 dilution of samples. Student's t-test (two tailed) was performed for significance.

Statistics

All data were analyzed using GraphPad Prism v5.0 for live cell image analysis or v7.0 software for all other analyses. Briefly, D'Agostino-Pearson tests were used to determine normality. Brown-Forsthe/Barlett's tests were used to determine equal variance for ANOVA

and F-test was used to determine equal variance for t-test in GraphPad Prism v7.0 software. Data that passed normality tests and equal variance tests were analyzed by t-test for two groups or ANOVA for three or more groups. Data that were not normally distributed were analyzed by Kruskal-Wallis test (three or more groups). Post-hoc analysis for multiple comparisons were selected as appropriate to test for statistical significance; * $p < 0.05$, ** $p < 0.01$, ***$p<0.001$. Results are presented as mean ± SEM.

RESULTS

Caveolae are specialized plasma membrane domains that facilitate interactions between signaling proteins (i.e. Gq, PLC, Src, etc[12,48,49]) and membrane receptors (i.e. α-adrenergic receptors[49]). These structures are found in endothelium and smooth muscle; however, their signaling functions are much less studied in smooth muscle. In electron micrographs, we consistently observe caveolae contained in arteriolar smooth muscle in proximity to sympathetic nerves (Supplemental Figure I). For this reason, we hypothesized that the caveolin-1 protein, the main component to caveolae, may associate with Panx1, which is activated in response to adrenergic stimulation.

In initial experiments, we performed live-cell confocal microscopy using *in vitro* human VSMC culture systems to measure the distribution and co-localization of exogenously expressed RFP-tagged Panx1 and GFP-tagged caveolin-1 following phenylephrine stimulation (Figure 1A). Baseline fluorescence measurements were recorded for 2 min prior to stimulation with phenylephrine (100 μmol/L), vehicle control, or high concentration ATP (500 μmol/L) to promote Panx1 internalization. A strong and significant co-distribution was observed between caveolin-1 and Panx1 at 30 seconds of phenylephrine stimulation at the plasma membrane (Figure 1A–B), which persisted above control fluorescence, although not to statistically significant levels (Figure 1B–C). Conversely, treatment with high-concentration ATP caused a significant and continuous reduction in co-localized signal, consistent with internalization and loss of Panx1 on the cell surface[50,51] that is independent of caveolin-1 mediated endocytosis[43]. Vehicle control-treated cells showed no changes in fluorescence co-localization from baseline.

To confirm observations from live-cell imaging experiments, we next performed *in vitro* cell fractionation and co-immunoprecipitation assays using *in vitro* VSMC culture systems to probe for endogenous interactions between Panx1 and caveolin-1 at the plasma membrane. We found that caveolin-1 and Panx1 localize to membrane-associated fractions (Figure 1D) and specifically overlap in caveolin-1-enriched sucrose-gradient fractions, suggesting partial localization of Panx1 to lipid microdomains containing caveolin-1 (Figure 1E). To determine if caveolin-1 and Panx1 interact following adrenergic stimulation, we acutely treated VSMCs with phenylephrine (20 μmol/L). Fractions enriched or deficient in caveolin-1 were isolated and Panx1 was precipitated using a protein specific antibody[45]. We found that caveolin-1 from enriched fractions significantly co-precipitated with Panx1 after adrenergic stimulation (Figure 1F), suggesting that plasma membrane complexes containing caveolin-1 and Panx1 form following adrenergic stimulation and may act to facilitate channel function.

Panx1-mediated ATP release and subsequent vasoconstriction are specifically mediated through α-AR activation[21,22,29–31]. Based on our initial observations and the *in vitro* biochemical findings herein (Figure 1F), we first tested if caveolin-1 and Panx1 similarly interact in VSMCs of *ex-vivo* isolated mouse resistance arteries. We performed proximity ligation assays (PLA) between Panx1 and caveolin-1 on TDAs and assessed the focal plane where sympathetic nerves innervate VSMC (Supplemental Figure II). Sympathetic nerves were specifically labeled with tyrosine hydroxylase. In control experiments using PLA secondary antibodies alone or IgG controls, we could not detect PLA punctate signals (red puncta indicate protein associations when PLA probes <40nm in apposition) – only sympathetic nerves could be viewed (Figure 2A–B). Next, we performed PLA for caveolin-1 and Panx1. Here we observed relatively few positive red punctate signals under control conditions (Figure 2C); however, following acute (1 min) phenylephrine stimulation (20 μmol/L), we observed an induction of PLA signal, which predominantly localized at the VSMC plasma membrane near areas of sympathetic nerve innervation (Figure 2D–E). As a control, TDA smooth muscle and sympathetic nerves were also analyzed for Cx43 expression, but it was not detected (Supplemental Figure III). The neuronal vesicular nucleotide transporter (VNUT) was also analyzed, but was only observed in sympathetic nerves, and not VSMCs as anticipated (Supplemental Figure III). These data demonstrate the formation of potential signaling microdomains where caveolin-1 and Panx1 are recruited together following adrenergic stimulation.

To investigate the functional and physiological role of VSMC caveolin-1 during α-AR vasoconstriction, we generated an inducible, VSMC-specific caveolin-1 knockout mouse model (SMC-Cav1$^{fl/fl}$), which upon induction of Cre recombinase deletes exon 2 of caveolin-1 (SMC-Cav1$^{Δ/Δ}$) (Figure 3A–B). Caveolin-1 deletion was specific for VSMCs of resistance arteries, not affecting caveolin-1 expression in CD31 positive endothelial cells (Figure 3C–D). Due to the well-established contribution of Panx1-mediated ATP release during adrenergic stimulation[21,22,29,52], we measured vasoconstrictor-dependent ATP release from isolated resistance arteries. Using a luminescence-based assay, we observed a caveolin-1 dependent response, whereby ATP released following adrenergic stimulation (norepinephrine 20 μmol/L or phenylephrine 20 μmol/L) was significantly reduced in SMC-Cav1$^{Δ/Δ}$ mice compared with controls (Figure 3E). No significant effect on ATP release was observed in any of the genotypes tested in response to agonists for other potent vasoconstriction pathways (e.g., ET-1 or 5-HT) (Figure 3E). Intracellular ATP concentration was also unchanged in any of the genotypes tested (Supplemental Figure IV).

In line with our ATP findings, we reasoned that blunted adrenergic-mediated ATP release in SMC-Cav1$^{Δ/Δ}$ mice would concomitantly impair vascular responses to phenylephrine. To directly measure vasoconstriction responses in *ex vivo* resistance arteries, we assessed vascular responses to increasing concentrations of phenylephrine using pressure myography. SMC-Cav1$^{Δ/Δ}$ mice exhibited significant reductions in phenylephrine-stimulated vasoconstriction (red line) compared with control animals (black line) (Figure 4A). Unlike global caveolin-1 knockout mice, which exhibit reduced expression of endothelial cell caveolin-1[16,53], no significant differences were observed in endothelium-dependent vasodilation (acetylcholine responses) in SMC-Cav1$^{Δ/Δ}$ mice (Figure 4B). Thus, VSMC-

specific deletion of caveolin-1 impairs adrenergic vasoconstriction without altering endothelial-mediated responses.

Previously we have shown that VSMC-specific deletion of Panx1 channels results in significantly reduced BP due to blunted adrenergic-stimulated ATP release and vasoconstriction. Thus, we used telemetry to test whether SMC-Cav1$^{\Delta/\Delta}$ mice exhibited a similar BP phenotype. BP was assessed in individual animals before (baseline) and after induction of caveolin-1 deletion. A significant reduction in 24-hour mean arterial pressure (total MAP= −3.8 mmHg) was observed only after tamoxifen injection in SMC-Cav1$^{\Delta/\Delta}$ mice (Figure 5A–B). Moreover, a significant and greater BP reduction (ΔMAP= −6.8 mmHg) was observed during the active period, when sympathetic drive to resistance arteries is higher (Figure 5C) compared to the inactive period (Figure 5D). No significant difference in baseline MAP was observed in any other tested genotype before induction with tamoxifen, vehicle control, or saline control (Figure 5C; Supplemental Figure V). There was also no change in plasma renin concentration after caveolin-1 deletion, which was tested as a metric of altered basal renal-vasculature function (Supplemental Figure V).

To ensure that BP reductions in SMC-Cav1$^{\Delta/\Delta}$ mice were not influenced by changes in cardiac function, we performed functional MRI analysis on SMC-Cav1$^{\Delta/\Delta}$ and control animals (Figure 6). No significant changes in cardiac function were observed in any of the tested genotypes (Table 1). This includes cardiovascular changes due to heart rate, stroke volume, cardiac output, left ventricular mass, or left ventricular wall thickness–all of which can directly influence MAP. Lastly, mice lacking the Cre allele, but maintaining the loxP genotype and injected with tamoxifen, showed no changes in expression of caveolin-1 in arteries, phenylephrine dose-responses, or MRIs (Supplemental Figure VI; Supplemental Table I).

To functionally assess whether BP reductions involving VSMC caveolin-1 are mediated through a Panx1-dependent pathway, we acutely treated animals with the Panx1 intracellular loop mimetic peptide-inhibitor PxIL2P (20 mg/kg) or scrambled control peptide (20 mg/kg). We have previously shown that PxIL2P significantly blunts phenylephrine-stimulated Panx1-channel currents, ATP release, vasoconstriction, and MAP[22]. Following acute injection of PxIL2P, significant BP reduction was restricted to vehicle treated SMC-Cav1$^{fl/fl}$ (vehicle treated: ΔMAP= −8.83 mmHg) and C57BL/6 (vehicle treated: ΔMAP= −12.26 mmHg; tamoxifen; ΔMAP= −9.81 mmHg) control animals–both of which contain VSMC caveolin-1. Conversely, no significant changes in MAP were observed in SMC-Cav1$^{\Delta/\Delta}$ animals, which are deficient in VSMC caveolin-1 (tamoxifen: ΔMAP= 0.73 mmHg; Figure 7). Administration of a scrambled PxIL2P peptide of the same amino acid composition did not influence BP in any genotype tested. The resistance of VSMC-specific caveolin-1 deficient mice to BP lowering by PxIL2P supports the idea that VSMC caveiolin-1 regulates BP homeostasis through changes in Panx1 localization and channel function.

DISCUSSION

Sympathetic-mediated vasoconstriction plays a central role in controlling BP homeostasis. This process occurs in part due to the release of norepinephrine from sympathetic nerves,

subsequent activation of VSMC α-ARs, and coordinated constriction between VSMCs, thus producing a unified vasoconstriction response. Recent work from our group revealed that VSMC Panx1 channels[21] are a primary mediator of α-AR vasoconstriction, and using VSMC-specific Panx1 knockout mice and genetic rescue experiments we demonstrated that ATP release from tehse channels was necessary for proper adrenergic vasoconstriction[21,54]. In this way, ATP acts as an autocrine/paracrine signaling molecule that initiates vasoconstriction responses in resistance arteries. However, less is known about the intracellular signaling molecules responsible for supporting Panx1 channel function following adrenergic stimulation. Here we have identified a novel interaction between Panx1 and the caveolae structural protein caveolin-1. Caveolin-1 and Panx1 localize to areas of the plasma membrane innervated by sympathetic nerves and associate with each other following stimulation of α-ARs with phenylephrine. Using a novel, inducible, VSMC-specific caveolin-1 knockout mouse, we also demonstrate that caveolin-1 functionally regulates adrenergic-mediated ATP release, vasoconstriction, MAP, and Panx1 dependent BP responses.

Plasma membrane caveolae influence vascular homeostasis and assist in the localization of key VSMC vasoconstriction signaling molecules such as α-AR and Gq coupled effector molecules in small arteries[19,49,55]. From electron microscopy observations (Supplemental Figure I), we often observe caveolae localized near sympathetic nerves, and thus predicted that this unique vascular feature may beget vascular function. Our live cell, fluorescent tracking experiments, allowed us to examine caveolin-1 and Panx1 interactions in response to stimulation with phenylephrine. Activation of α-AR resulted in a rapid co-association of the two proteins at the plasma membrane (Figure 1A–B). These temporal effects are consistent with previous constriction recordings following adrenergic stimulation in resistance arteries[56,8]. Moreover, we treated VSMCs with a high concentration of ATP (500 μmol/L), a manipulation that promotes active internalization of membrane associated Panx1[50], to determine if caveolin-1 association correlates with Panx1 endocytosis. Here we observed a significant decrease in co-localization between Panx1 and caveolin-1 following ATP stimulation (Figure 1A–C), indicating that Panx1 endocytosis occurs independently of a caveolin-1 association.

Recent studies by Boyce et al.[50] and Gehi et al.[43] report similar co-distributions of Panx1 with caveolin-1 in cell lines. In contrast to the phenylephrine-induced Panx1/caveolin-1 clustering observed herein, a similar decrease in overlap with caveolin-1 was observed following ATP application in N2a cells.[50] It is important to note in this context that caveolin-1-enriched caveolae are only one specialized variety of cholesterol-enriched membrane microdomain or lipid raft[5]. In fact, ATP-mediated Panx1 internalization is cholesterol-dependent[50,51] but dynamin- and clathrin-independent[43,50], suggestive of a non-canonical endocytosis mechanism. Our novel results then suggest that inclusion of Panx1 in VSMC caveolae may alter channel activity (such as increased open probability[57–59]) rather than trafficking, although this remains to be explicitly tested. In light of this work, and because of the strong association between caveonlin-1 and Panx1 following adrenergic stimulation, we tested whether an endogenous interaction occurs in VSMCs. The same culture model also showed a specific protein interaction using immunoprecipitation of membrane fractions after phenylephrine stimulation (Figure 1D–F), which was absent in

non-caveolar Panx1-containing fractions. In these experiments, we observed multiple glycosylation species of Panx1[60,61] (between 37–55kDa) after immunoprecipitation, perhaps indicative of the recruitment of more Panx1 channels from intracellular stores following stimulation. Panx1 channels are oligomers of Panx1 subunits. It is unknown how many units within the channel must be glycosylated to allow for the appropriately trafficking of plasma membrane channels. It is plausible that Panx1 subunits are differentially regulated, which has been strongly suggested in other published work[29]. It also remains to unknown whether binding of Panx1 to caveolin-1 after phenylephrine stimulation requires a direct interaction, which has been observed for other membrane channels[57–59], or if other membrane associated effector molecules are required, such as Src family kinases[62,63].

Panx1 plays a vital role in α–AR vasoconstriction, but not in other constriction pathways[22]. We reasoned that caveolae might engender the formation of α–AR membrane microdomains near the VSMC membrane innervated by sympathetic nerves. Using intact mouse resistance arteries in conjunction with PLA, we observed an adrenergic-induced interaction of caveolin-1 and Panx1 preferentially localized around sympathetic nerves (Figure 2D–E). These observations suggest that caveolae may support the formation of a signaling microdomain important for Panx1 activation[22]. Moreover, resistance arteries are characterized by multiunit neural innervation to VSMCs, whereby small patches of VSMCs are contacted by sympathetic nerves to allow for finer individual control of vasoconstriction[64]. This innervation pattern differs from the unitary innervation observed in visceral organs and large arteries, which features a single VSMC neural input and relies on gap junction connectivity to synchronize constriction responses. In this study as in previously published findings [21], we detect a scarcity of gap junction connectivity between VSMCs in our models by Cx43 immunostaining herein (Supplemental Figure III) or electron microscopy[21]. These results suggest that resistance arteries may preferentially utilize autocrine/paracrine-mediated signals to couple VSMC constriction responses, and may further utilize purinergic signaling pathways mediated through Panx1 to facilitate this function.

The idea that spatially localized signals support vascular function has been extensively characterized in the endothelium, where regulation of tyrosine kinases and endothelial nitric oxide synthase is dependent on caveolin-1[5]; however, less is known about these processes in VSMCs, which utilize sympathetic innervation to adjust vascular resistance for proper blood pressure control[65]. Perturbations to this adrenergic signaling axis may underlie clinical pathologies in patients suffering from treatment-resistant hypertension who present with enhanced sympathetic drive, norepinephrine spillover, and excessive vascular resistance[66–68].

To explore the functional role of caveolin-1 in VSMCs we generated an inducible VSMC-specific caveolin-1 knockout mouse (Figure 3A–B) to selectively removed caveolin-1 from the vascular media (Figure 3C). Importantly, caveolin-1 expression remained present in the vascular endothelium (CD31-positive cells) between control and knockout mice. No gross alterations in the medial wall thickness or cell number were observed in TDAs (data not shown) as was described for pulmonary arteries in the constitutive global knockout[13]. It is

likely that the utilization of an inducible Cre-recombinase system in adult mice curtailed any negative compensatory effects seen in constitutive systems.

Using ATP bioluminescence assays, we measured phenylephrine-stimulated ATP release from *ex vivo* arteries, a process that our laboratory has shown uniquely couples with Panx1 activation[22]. In all cases, caveolin-1 deletion significantly reduced phenylephrine- and norepinephrine-stimulated ATP release, similar to observations in Panx1 VSMC-knockout mice[22] (Figure 3E). From our immunofluorescence analyses, it seems likely that Panx1 is the primary conduit for ATP release from VSMCs, as VNUT and Cx43 were not detected in VSMCs of our vessels (Supplemental Figure III). These data suggest that caveolin-1 is involved upstream of Panx1 activation and influences the ATP release typically ascribed to Panx1 function. It remains to be demonstrated if a direct interaction between caveolin-1 is sufficient to induce Panx1 channel opening.

In the vasculature, a primary role for caveolin-1 is ascribed to negative regulation of endothelial nitric oxide synthase (eNOS) activity in the endothelium[69,70]. Global deletion of caveolin-1 increases eNOS activity, resulting in higher concentrations of cGMP, increased NO release, and alterations in myogenic tone and dilation responses to acetylcholine[16,53]. However, the role of VSMC-derived caveolin-1 has not been specifically examined in resistance arteries. Using pressure myography, we found that VSMC caveolin-1 deletion significantly blunts phenylephrine-stimulated vasoconstriction responses, but does not change vasodilation responses to acetylcholine (Figure 4A–B), indicating that reduced vasoconstriction is not dependent on endothelial-derived mechanisms observed in global caveolin-1 knockout models[13]. ATP release from the vascular wall exhibits dual activities in resistance arteries dependeing on which cell type release ATP (vasoconstriction in smooth muscles and vasodilation in endothelial cells) The subtypes of purinergic receptors that are activated by ATP can also influence responses within the vascular wall with the largest contribution in smooth muscle being mediated by P2X1 ionotropic receptors[71]. Our laboratory has demonstrated the existence of purinergic component to adrenergic mediated vascular events whereby incubation of vessels with the ATP degrading enzyme apyrase or pharmacological blockers of purinergic receptors (P2X) prevents adrenergic vasoconstriction[21]. Thus, we conclude that caveolin-1 in our model functionally regulates the initial and upstream release of ATP utilized to activate downstream purinergic receptors after adrenergic stimulation.

VSMC-specific deletion of caveolin-1 results in reduced adrenergic ATP release and vasoconstriction, a similar vascular phenotypic observed when Panx1 is specifically deleted from VSMCs. We predicted that a similar dysregulation in BP would then occur after caveolin-1 deletion as observed in Panx1 knockout models: specifically, a reduction in MAP predominantly during the animal's active period (night MAP), when sympathetic drive is high. Indeed, *in vivo* BP monitoring revealed a significant reduction in 24 hour MAP (Figure 5A–B) with a greater reduction occurring at night (Figure 5C) in caveolin-1-deficient animals, but not during the day (inactive period) (Figure 5D). The effect size of BP lowering due to caveolin-1 deletion (~4 mmHg, 24 hour MAP; ~6 mmHg, Night MAP) was nearly identical to BP reductions in VSMC-Panx1 knockout animals[53]. To further confirm that alterations in MAP were due to vascular changes (reduced vascular resistance), we assessed

cardiac function using MRI. No measurable morphological differences were detected in our analysis and all animals were functionally similar (e.g., heart rate, stroke volume; Table 1). Therefore, alterations in vascular resistance due to VSMC caveolin-1 deletion are likely responsible for observed reductions in MAP.

To determine if caveolin-1 dependent BP responses utilize in part a Panx1-dependent pathway, we acutely treated animals with PxIL2P peptide to pharmacologically lower blood pressure. PxIL2P has previously been shown to significantly reduce adrenergic stimulated Panx1 channel opening and ATP release, and also potently lowers blood pressure in mice. In the current analysis, wild-type and control mice dramatically respond to PxIL2P treatment (i.e reduced blood pressure lowering), with no effects due to scrambled control peptide[22]. However, conditional deletion of VSMC caveolin-1 are completely protected to BP lowering by PxIL2P treatment. This strongly suggests that caveolin-1 is a key intermediary necessary for normal Panx1 function (Figure 7). These data further highlight the Panx1 intracellular loop as an important target for Panx1 activation. Previous work from our group has demonstrated that the region mapping to the PxIL2P peptide contains a regulatory motif, which upon genetic mutation negatively influences Panx1 channel function and adrenergic mediated vasoconstriction[22]. Future studies are needed to determine if caveolin-1 directly influences the Panx1 intracellular loop, or if associative factors bound to caveolin-1 are required for proper channel function.

In this analysis, we explore a novel adrenergic vasoconstriction pathway that has previously been shown to coordinate constriction responses through the release of ATP by Panx1. We describe the impact of caveolin-1 deletion in the peripheral vasculature and on systemic BP regulation using a novel smooth muscle-specific mouse model. We have limited changes due to compensatory deletion-effects by utilizing an inducible Cre-lox system in adult mice. Based on our analyses we found no additional phenotypes outside of the cardiovascular phenotypes reported in this study. Although, direct experimental evidence and future studies are required to determine if additional phenotypes exist. Here we show that the localization of Panx1 to plasma membrane caveolae and the scaffold protein caveolin-1 promotes a novel interaction important for regulating BP. It remains to be observed whether other scaffold proteins or cytoskeletal proteins contribute to the localization and formation of this unique membrane domain near sympathetic nerve terminals in VSMC. Panx1 has been shown to directly interact with the actin cytoskeleton[72] and its modulator actin-related protein 3[73,74], and treatment with cytochalasin B destabilized Panx1 plasma membrane distribution *in vitro*[72]. It is also unknown which intracellular mediators are mechanistically required for activation of Panx1 by α-AR in VSMCs, which will be especially important to determine.

Overall, our data demonstrate that Panx1 and caveolin-1 functionally couple with each other in VSMCs. Using immunofluorescence co-localization and co-immunoprecipitation, we show that caveolin-1 and Panx1 interact at distinct areas of VSMC plasma membrane innervated by sympathetic nerves, suggesting the existence of an adrenergic micro-signaling domain. This interaction was induced by α-AR stimulation and is necessary for adrenergic-mediated vasoconstriction and ATP release from resistance arteries. We found that VSMC caveolin-1 is necessary to control systemic BP responses through modulation of Panx1

function and may facilitate appropriate channel function through the Panx1 intracellular loop region.

Supplementary Material

Refer to Web version on PubMed Central for supplementary material.

Acknowledgments

We would like to thank Dr. Chen Li (formerly at University of Virginia) for the kind gift of VNUT antibody, and the Advanced Microscopy Facility for assistance with processing samples for electron microscopy. We would also like to acknowledge the University of Virginia Histology core for processing vessels for sectioning and mounting, and the University of Virginia MRI core for mouse imaging.

SOURCE OF FUNDING: This study was supported by the National Institutes of Health HL007284 (LJD and MEG), HL137270 (LJD), HL131399 (MEG), HL120840 (BEI), American Heart Association predoctoral fellowships (ASK and TCSK), the CFI 29462 (LAS), the BCKDF 804754 (LAS), Michael Smith Foundation for Health Research (LAS) and BC Schizophrenia Society Foundation Scholar Award 5900 (LAS), and NSERC 402270-2011 (LAS).

NON-STANDARD ABBREVIATIONS AND ACRONYMS

Panx1	Pannexin 1
VSMC	Vascular smooth muscle cell
BP	Blood pressure
MAP	Mean arterial pressure
TDA	Thoracodorsal artery
PE	Phenylephrine
α–AR	α–adrenergic receptor
VNUT	Vesicular nucleotide transporter
Cx43	Connexin43
Cav1	Caveolin-1

References

1. Christensen KL, Mulvany MJ. Location of resistance arteries. Journal of vascular research. 2001; 38(1):1–12.
2. Tanoue A, Nasa Y, Koshimizu T, et al. The alpha(1D)-adrenergic receptor directly regulates arterial blood pressure via vasoconstriction. The Journal of clinical investigation. 2002; 109(6):765–775. [PubMed: 11901185]
3. Bennett MR. Autonomic neuromuscular transmission at a varicosity. Progress in neurobiology. 1996; 50(5–6):505–532. [PubMed: 9015825]
4. Burnstock G, Ralevic V. Purinergic Signaling and Blood Vessels in Health and Disease. Pharmacological Reviews. 2013; 66(1):102–192. [PubMed: 24335194]
5. Caveolae Sowa G, Caveolins Cavins. Endothelial Cell Function: New Insights. Frontiers in Physiology. 2012; 2(120)

6. Rahman A, Swärd K. The role of caveolin-1 in cardiovascular regulation. Acta physiologica (Oxford, England). 2009; 195(2):231–245.
7. Li X-A, Everson WV, Smart EJ. Caveolae, Lipid Rafts, and Vascular Disease. Trends in Cardiovascular Medicine. 2005; 15(3):92–96. [PubMed: 16039968]
8. Martínez-Salas SG, Campos-Peralta JM, Pardo JP, et al. α1D-Adrenoceptor regulates the vasopressor action of α1A-adrenoceptor in mesenteric vascular bed of α1D-adrenoceptor knockout mice. Autonomic and Autacoid Pharmacology. 2011; 31(3–4):64–71. [PubMed: 21951586]
9. Predescu D, Vogel SM, Malik AB. Functional and morphological studies of protein transcytosis in continuous endothelia. American Journal of Physiology-Lung Cellular and Molecular Physiology. 2004; 287(5):L895–901. [PubMed: 15475492]
10. Williams TM, Lisanti MP. Caveolin-1 in oncogenic transformation, cancer, and metastasis. AJP: Cell Physiology. 2005; 288(3):C494–506. [PubMed: 15692148]
11. Patel HH, Murray F, Insel PA. G-Protein-Coupled Receptor-Signaling Components in Membrane Raft and Caveolae Microdomains. In: Klussmann E, Scott J, editorsProtein-Protein Interactions as New Drug Targets. Berlin, Heidelberg: Springer Berlin Heidelberg; 2008. 167–184.
12. Parton RG, del Pozo MA. Caveolae as plasma membrane sensors, protectors and organizers. Nature Reviews Molecular Cell Biology. 2013; 14(2):98–112. [PubMed: 23340574]
13. Drab M, Verkade P, Elger M, et al. Loss of caveolae, vascular dysfunction, and pulmonary defects in caveolin-1 gene-disrupted mice. Science. 2001; 293(5539):2449–2452. [PubMed: 11498544]
14. Fra AM, Williamson E, Simons K, Parton RG. De novo formation of caveolae in lymphocytes by expression of VIP21-caveolin. Proceedings of the National Academy of Sciences of the United States of America. 1995; 92(19):8655–8659. [PubMed: 7567992]
15. Razani B, Combs TP, Wang XB, et al. Caveolin-1-deficient mice are lean, resistant to diet-induced obesity, and show hypertriglyceridemia with adipocyte abnormalities. Journal of Biological Chemistry. 2002; 277(10):8635–8647. [PubMed: 11739396]
16. Razani B, Lisanti MP. Caveolin-deficient mice: insights into caveolar function human disease. The Journal of clinical investigation. 2001; 108(11):1553–1561. [PubMed: 11733547]
17. Albinsson S, Shakirova Y, Rippe A, et al. Arterial remodeling and plasma volume expansion in caveolin-1-deficient mice. American Journal of Physiology-Regulatory, Integrative and Comparative Physiology. 2007; 293(3):R1222–R1231.
18. Bernatchez P, Sharma A, Bauer PM, Marin E, Sessa WC. A noninhibitory mutant of the caveolin-1 scaffolding domain enhances eNOS-derived NO synthesis and vasodilation in mice. The Journal of Clinical Investigation. 2011; 121(9):3747–3755. [PubMed: 21804187]
19. Morris JB, Huynh H, Vasilevski O, Woodcock EA. α1-Adrenergic receptor signaling is localized to caveolae in neonatal rat cardiomyocytes. Journal of molecular and cellular cardiology. 2006; 41(1):17–25. [PubMed: 16730745]
20. Hardin CD, Vallejo J. Caveolins in vascular smooth muscle: form organizing function. Cardiovascular research. 2006; 69(4):808–815. [PubMed: 16386721]
21. Billaud M, Lohman AW, Straub AC, et al. Pannexin1 Regulates 1-Adrenergic Receptor-Mediated Vasoconstriction. Circulation Research. 2011; 109(1):80–85. [PubMed: 21546608]
22. Billaud M, Chiu Y-H, Lohman AW, et al. A molecular signature in the Pannexin 1 intracellular loop confers channel activation by the α1-adrenergic receptor in smooth muscle cells. Science Signaling. 2015:1–63.
23. Baek PJ, Sung-Jin K. Anti-hypertensive effects of probenecid via inhibition of the α-adrenergic receptor. Pharmacological Reports. 2011; 63(5):1145–1150. [PubMed: 22180356]
24. Nyberg M, Piil P, Kiehn OT, et al. Probenecid Inhibits α-Adrenergic Receptor–Mediated Vasoconstriction in the Human Leg VasculatureNovelty and Significance. Hypertension. 2018; 71(1):151–159. [PubMed: 29084879]
25. Adamson SE, Leitinger N. The role of pannexin1 in the induction and resolution of inflammation. FEBS letters. 2014; 588(8):1416–1422. [PubMed: 24642372]
26. Sandilos JK, Chiu YH, Chekeni FB, et al. Pannexin 1, an ATP release channel, is activated by caspase cleavage of its pore-associated C-terminal autoinhibitory region. J Biol Chem. 2012; 287(14):11303–11311. [PubMed: 22311983]

27. Chekeni FB, Elliott MR, Sandilos JK, et al. Pannexin 1 channels mediate 'find-me' signal release and membrane permeability during apoptosis. Nature. 2010; 467(7317):863–867. [PubMed: 20944749]
28. Lohman AW, Billaud M, Straub AC, et al. Expression of pannexin isoforms in the systemic murine arterial network. Journal of vascular research. 2012; 49(5):405–416. [PubMed: 22739252]
29. Chiu Y-H, Jin X, Medina CB, et al. A quantized mechanism for activation of pannexin channels. Nature Communications. 2017; 8:1–15.
30. Angus JA, Wright CE. Novel α 1-adrenoceptor antagonism by the fluroquinolone antibiotic trovafloxacin. European journal of pharmacology. 2016; 791:179–184. [PubMed: 27590356]
31. Kauffenstein G, Tamareille S, Prunier F, et al. Central role of P2Y6 UDP receptor in arteriolar myogenic tone. Arteriosclerosis, thrombosis, and vascular biology. 2016 ATVBAHA-116.
32. Lohman AW, Billaud M, Isakson BE. Mechanisms of ATP release and signalling in the blood vessel wall. Cardiovascular Research. 2012; 95(3):269–280. [PubMed: 22678409]
33. Wirth A, Benyó Z, Lukasova M, et al. G12-G13-LARG-mediated signaling in vascular smooth muscle is required for salt-induced hypertension. Nature Medicine. 2008; 14(1):64–68.
34. Cao G, Yang G, Timme TL, et al. Disruption of the caveolin-1 gene impairs renal calcium reabsorption and leads to hypercalciuria and urolithiasis. The American journal of pathology. 2003; 162(4):1241–1248. [PubMed: 12651616]
35. Han M, Dong L-H, Zheng B, Shi J-H, Wen J-K, Cheng Y. Smooth muscle 22 alpha maintains the differentiated phenotype of vascular smooth muscle cells by inducing filamentous actin bundling. Life sciences. 2009; 84(13):394–401. [PubMed: 19073196]
36. Zimmermann O, Zwaka TP, Marx N, et al. Serum starvation and growth factor receptor expression in vascular smooth muscle cells. Journal of vascular research. 2006; 43(2):157–165. [PubMed: 16407661]
37. Ma X, Wang Y, Stephens NL. Serum deprivation induces a unique hypercontractile phenotype of cultured smooth muscle cells. American Journal of Physiology-Cell Physiology. 1998; 274(5):C1206–C1214.
38. Straub AC, Lohman AW, Billaud M, et al. Endothelial cell expression of haemoglobin α regulates nitric oxide signalling. Nature. 2012; 491(7424):473–477. [PubMed: 23123858]
39. Billaud M, Lohman AW, Straub AC, Parpaite T, Johnstone SR, Isakson BE. Characterization of the thoracodorsal artery: morphology and reactivity. Microcirculation. 2012; 19(4):360–372. [PubMed: 22335567]
40. Straub AC, Butcher JT, Billaud M, et al. Hemoglobin alpha/eNOS Coupling at Myoendothelial Junctions Is Required for Nitric Oxide Scavenging During Vasoconstriction. Arterioscler Thromb Vasc Biol. 2014; 34(12):2594–2600. [PubMed: 25278292]
41. Penuela S, Bhalla R, Gong X-Q, et al. Pannexin 1 and pannexin 3 are glycoproteins that exhibit many distinct characteristics from the connexin family of gap junction proteins. Journal of Cell Science. 2007; 120(Pt 21):3772–3783. [PubMed: 17925379]
42. Schindelin J, Arganda-Carreras I, Frise E, et al. Fiji: an open-source platform for biological-image analysis. Nature methods. 2012; 9(7):676. [PubMed: 22743772]
43. Gehi R, Shao Q, Laird DW. Pathways regulating the trafficking and turnover of pannexin1 protein and the role of the C-terminal domain. The Journal of biological chemistry. 2011; 286(31):27639–27653. [PubMed: 21659516]
44. Bolte S, Cordelieres FP. A guided tour into subcellular colocalization analysis in light microscopy. Journal of Microscopy. 2006; 224(3):213–232. [PubMed: 17210054]
45. Penuela S, Gehi R, Laird DW. The biochemistry and function of pannexin channels. Biochimica et biophysica acta. 2013; 1828(1):15–22. [PubMed: 22305965]
46. Billaud M, Lohman AW, Straub AC, Parpaite T, Johnstone SR, Isakson BE. Characterization of the Thoracodorsal Artery: Morphology and Reactivity. Microcirculation. 2012; 19(4):360–372. [PubMed: 22335567]
47. Vandsburger MH, French BA, Helm PA, et al. Multi-parameter in vivo cardiac magnetic resonance imaging demonstrates normal perfusion reserve despite severely attenuated β-adrenergic functional response in neuronal nitric oxide synthase knockout mice. European heart journal. 2007; 28(22):2792–2798. [PubMed: 17602202]

48. Li S, Couet J, Lisanti MP. Src tyrosine kinases, Galpha subunits, and H-Ras share a common membrane-anchored scaffolding protein, caveolin. Caveolin binding negatively regulates the auto-activation of Src tyrosine kinases. Journal of Biological Chemistry. 1996; 271(46):29182–29190. [PubMed: 8910575]
49. Fujita T, Toya Y, Iwatsubo K, et al. Accumulation of molecules involved in α1-adrenergic signal within caveolae: caveolin expression and the development of cardiac hypertrophy. Cardiovascular research. 2001; 51(4):709–716. [PubMed: 11530104]
50. Boyce AKJ, Kim MS, Wicki-Stordeur LE, Swayne LA. ATP stimulates pannexin 1 internalization to endosomal compartments. The Biochemical journal. 2015; 470(3):319–330. [PubMed: 26195825]
51. Boyce AKJ, Swayne LA. P2X7 receptor cross-talk regulates ATP-induced pannexin 1 internalization. The Biochemical journal. 2017; 474(13):2133–2144. [PubMed: 28495860]
52. Chiu Y-H, Ravichandran KS, Bayliss DA. Intrinsic properties and regulation of Pannexin 1 channel. Channels. 2014; 8(2):103–109. [PubMed: 24419036]
53. Dubroca C, Loyer X, Retailleau K, et al. RhoA activation and interaction with Caveolin-1 are critical for pressure-induced myogenic tone in rat mesenteric resistance arteries. Cardiovascular research. 2007; 73(1):190–197. [PubMed: 17150200]
54. Billaud M, Chiu YH, Lohman AW, Parpaite T. A molecular signature in the pannexin1 intracellular loop confers channel activation by the α1 adrenoreceptor in smooth muscle cells. Science. 2015; 8(364):ra17–ra17.
55. Dreja K, Voldstedlund M, Vinten J. Cholesterol depletion disrupts caveolae and differentially impairs agonist-induced arterial contraction. Hypertension. 2002
56. Jackson WF, Boerman EM, Lange EJ, Lundback SS, Cohen KD. Smooth muscle alpha1D-adrenoceptors mediate phenylephrine-induced vasoconstriction and increases in endothelial cell Ca2+ in hamster cremaster arterioles. British Journal of Pharmacology. 2008; 155(4):514–524. [PubMed: 18604236]
57. Yeh Y-C, Parekh AB. Distinct structural domains of caveolin-1 independently regulate Ca2+ release-activated Ca2+ channels and Ca2+ microdomain-dependent gene expression. Molecular and cellular biology. 2015; 35(8):1341–1349. [PubMed: 25645930]
58. Kwiatek AM, Minshall RD, Cool DR, Skidgel RA, Malik AB, Tiruppathi C. Caveolin-1 regulates store-operated Ca2+ influx by binding of its scaffolding domain to TRPC1 in endothelial cells. Molecular pharmacology. 2006
59. Sundivakkam PC, Kwiatek AM, Sharma TT, Minshall RD, Malik AB, Tiruppathi C. Caveolin-1 scaffold domain interacts with TRPC1 and IP3R3 to regulate Ca2+ store release-induced Ca2+ entry in endothelial cells. AJP: Cell Physiology. 2008; 296(3):C403–C413. [PubMed: 19052258]
60. Penuela S, Lohman AW, Lai W, et al. Diverse post-translational modifications of the pannexin family of channel-forming proteins. Channels. 2014; 8(2):124–130. [PubMed: 24418849]
61. Penuela S, Bhalla R, Nag K, Laird DW. Glycosylation regulates pannexin intermixing and cellular localization. Molecular biology of the cell. 2009; 20(20):4313–4323. [PubMed: 19692571]
62. Grande-García A, Echarri A, de Rooij J, et al. Caveolin-1 regulates cell polarization and directional migration through Src kinase and Rho GTPases. The Journal of cell biology. 2007; 177(4):683–694. [PubMed: 17517963]
63. Gottlieb-Abraham E, Shvartsman DE, Donaldson JC, et al. Src-mediated caveolin-1 phosphorylation affects the targeting of active Src to specific membrane sites. Molecular biology of the cell. 2013; 24(24):3881–3895. [PubMed: 24131997]
64. Fisher SA. Vascular smooth muscle phenotypic diversity and function. Physiological Genomics. 2010; 42A(3):169–187. [PubMed: 20736412]
65. Fisher JP, Paton JFR. The sympathetic nervous system and blood pressure in humans: implications for hypertension. Journal of human hypertension. 2012; 26(8):463–475. [PubMed: 21734720]
66. Fisher JP, Young CN, Fadel PJ. Central sympathetic overactivity: maladies and mechanisms. Autonomic neuroscience : basic & clinical. 2009; 148(1–2):5–15. [PubMed: 19268634]
67. Pimenta E, Calhoun DA. Resistant Hypertension: Incidence, Prevalence, and Prognosis. Circulation. 2012; 125(13):1594–1596. [PubMed: 22379111]

68. Manolis AJ, Poulimenos LE, Kallistratos MS, Gavras I, Gavras H. Sympathetic overactivity in hypertension and cardiovascular disease. Current vascular pharmacology. 2014; 12(1):4–15. [PubMed: 23905597]

69. Ju H, Zou R, Venema VJ, Venema RC. Direct interaction of endothelial nitric-oxide synthase and caveolin-1 inhibits synthase activity. Journal of Biological Chemistry. 1997; 272(30):18522–18525. [PubMed: 9228013]

70. Feron O, Belhassen L, Kobzik L, Smith TW, Kelly RA, Michel T. Endothelial nitric oxide synthase targeting to caveolae specific interactions with caveolin isoforms in cardiac myocytes and endothelial cells. Journal of Biological Chemistry. 1996; 271(37):22810–22814. [PubMed: 8798458]

71. Burnstock G. Control of vascular tone by purines and pyrimidines. British Journal of Pharmacology. 2010; 161(3):527–529. [PubMed: 20880393]

72. Bhalla-Gehi R, Penuela S, Churko JM, Shao Q, Laird DW. Pannexin1 and pannexin3 delivery, cell surface dynamics, and cytoskeletal interactions. The Journal of biological chemistry. 2010; 285(12):9147–9160. [PubMed: 20086016]

73. Wicki-Stordeur LE, Swayne LA. Panx1 regulates neural stem and progenitor cell behaviours associated with cytoskeletal dynamics and interacts with multiple cytoskeletal elements. Cell communication and signaling : CCS. 2013; 11(1):62. [PubMed: 23964896]

74. Swayne LA. Powerful partnership: crosstalk between pannexin 1 and the cytoskeleton. 2014:1–4.

PERSPECTIVES

A strong medical need exists for an effective, safe, and innovative pharmacological therapy that promotes BP regulation and reduces the vasoconstriction that accompanies excessive sympathetic stimulation. Our observations demonstrating an adrenergic-mediated interaction between VSMC caveolin-1 with Panx1, and the subsequent caveonlin-1 dependent control of vascular responsiveness and blood pressure homeostasis, are important for expanding our knowledge of a novel adrenergic signaling pathway that may underlie treatment-resistant hypertension. In the future, our goal is to elucidate signaling partners involved forming functional adrenergic signaling microdomains and determine their applicability as targets for therapeutic intervention.

HIGHLIGHTS

- Presents a novel interaction between the ATP release channel Pannexin1 and the caveolae scaffolding protein caveolin-1, which is mediated by adrenergic stimulation.
- Demonstrates that conditional genetic deletion of caveolin-1 from smooth muscle cells recapitulates Pannexin1 vascular phenotypes.
- Demonstrates that smooth muscle cell caveolin-1 regulates adrenergic stimulated vascular constriction and mean arterial pressure.

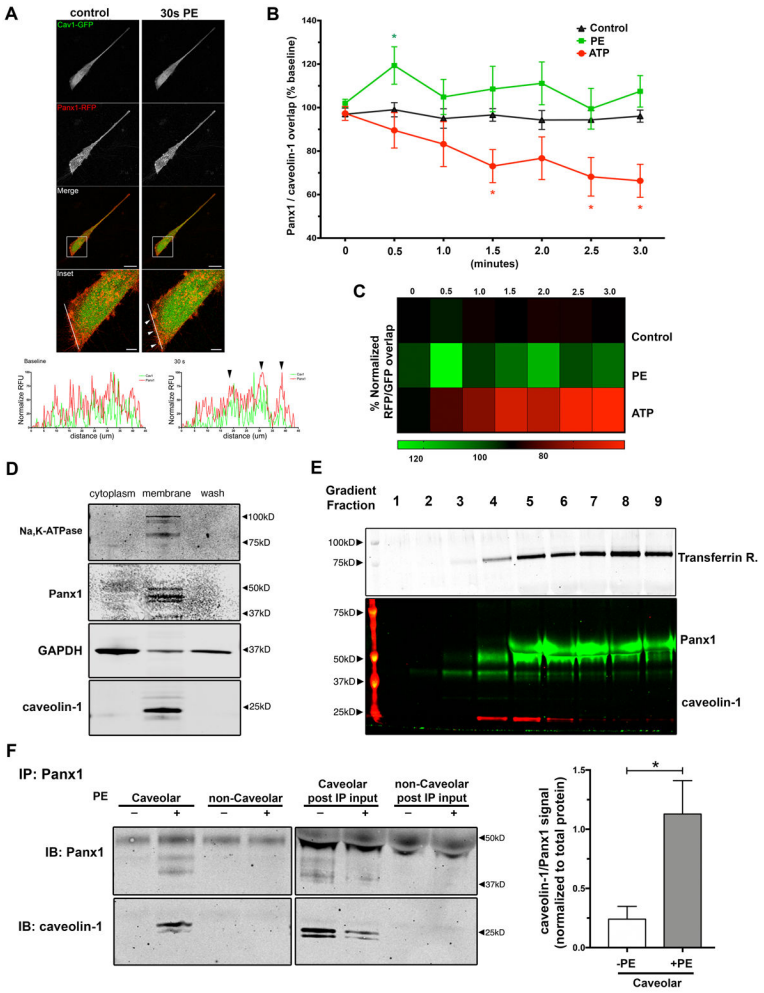

Figure 1. Pannexin 1 and caveolin-1 only associate after phenylephrine stimulation

(A) Confocal images and line scan analysis of cultured human VSMCs expressing Panx1-RFP and caveolin-1 GFP following phenylephrine stimulation. Scale bar; 50 μm (low-magnification) and 10 μm (high-magnification) **(B)** Co-localization analysis of continuous time lapse confocal imaging in human VSMCs throughout acute stimulation (total time= 3 min) with vehicle control (black line; n=11), 500 μmol/L ATP control (red line; n=5), or 100 μmol/L phenylephrine (green line; n=10). *p < 0.05 compared to vehicle control using two-way ANOVA with Dunnett's posthoc. (C) Heat map representation of percent fluorescence co-distribution using Mander's coefficient analysis and normalized to baseline (green=positive association; red=negative association). **(D)** Membrane fractionation and western analysis of VSMCs showing endogenous distribution of Panx1 and caveolin-1 in membrane fractions. **(E)** Subcellular distribution of caveolin-1 enriched membrane domains in sodium carbonate-based detergent-free cellular fractionation using a discontinuous sucrose gradient (5%–40%), analyzed by immunoblot. Panx1 co-fractionates with caveolin-1 in lipid light rafts at the plasma membrane. **(F)** Co-immunoprecipitation and quantification of Panx1 and caveolin-1 from subcellular plasma membrane domains was measured

following phenylephrine stimulation, n=5. Data analyzed by student's t-test and presented as mean ± SEM. * $p < 0.05$.

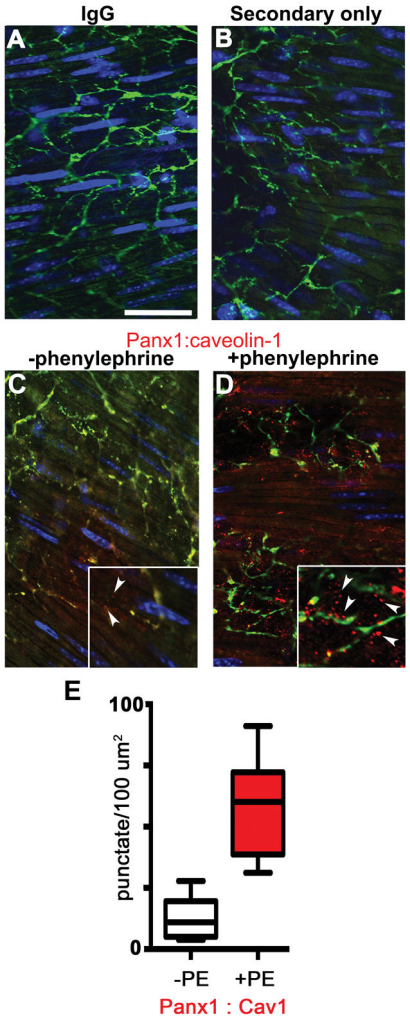

Figure 2. Pannexin1 and caveolin-1 localize to the plasma membrane near sympathetic nerves

En face immunofluorescence detection of Panx1 and caveolin-1 using proximity ligation assay (PLA) on intact TDA. Sympathetic nerves were labeled with tyrosine hydroxylase (green) and nuclei were labeled with DAPI (blue)**. (A)** Control IgG (rabbit) staining. **(B)** PLA secondary probe control. **(C)** Lack of positive PLA between Panx1 and caveolin-1 in VSMCs at baseline conditions. **(D–E)** Panx1 and caveolin-1 cluster at areas of sympathetic innervation following acute (1 min) phenylephrine treatment (20 μmol/L). Positive PLA amplification is visualized as red punctate spots (white arrows). **(E)** Quantification of PLA signal between Panx1 and caveolin-1 before and after treatment with phenylephrine. N=3 animals per treatment group. Scale bar; 50 μm.

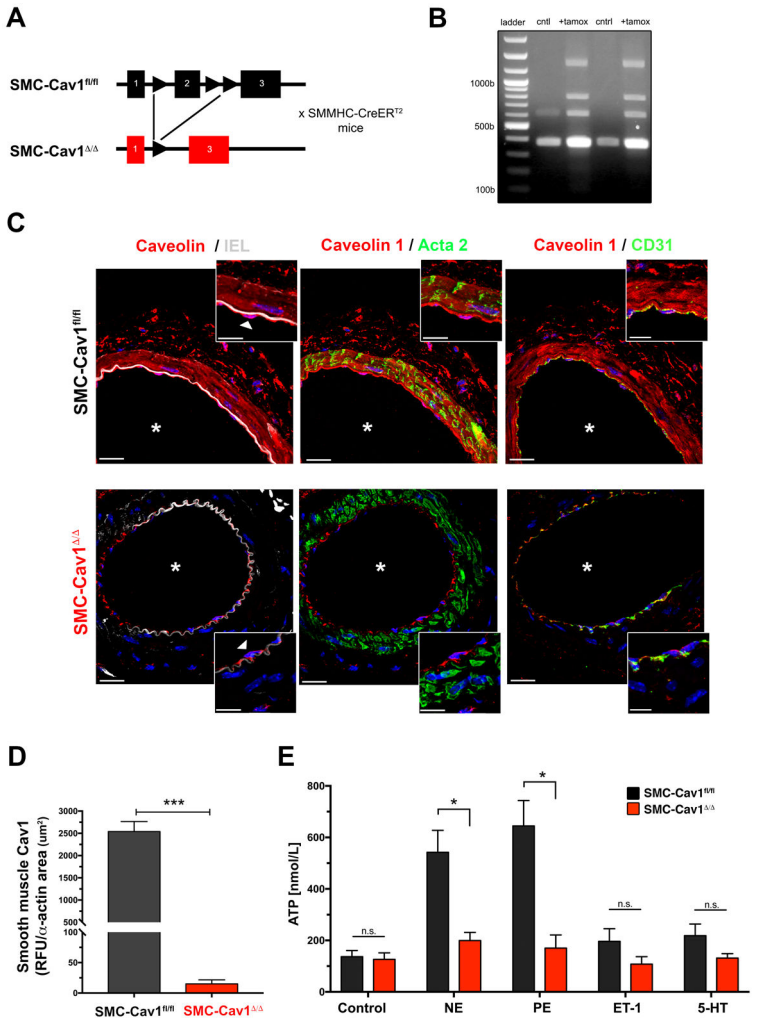

Figure 3. Inducible deletion of caveolin-1 from smooth muscle cells functionally mimics blunted adrenergic-mediated ATP release in Pannexin 1 deletion

(A) Inducible SMMHC-CreERT2+/Cav1fl/fl (SMC-Cav1fl/fl) mice were injected with tamoxifen (1 mg/kg) to delete caveolin-1 (SMC-Cav1Δ/Δ). (B) Agarose gel from genomic DNA showing Cre-mediated recombination at loxP site in tamoxifen treated mice. (C) Immunostaining of transverse sections of TDAs with anti-caveolin-1 (red), internal elastic lamina (gray), α-SMactin (Acta2), or CD-31 (Pecam1) (green). Nuclei are stained with DAPI (blue). *indicates vessel lumen. Scale bar; 20 μm. Arrows in high magnification indicate endothelial cells. (D) Quantification of caveolin-1 deletion from VSMCs normalized to α-SMactin positive area; n=6 mice. Students t-test was performed, significance indicated by asterisk ***$p < 0.001$. (E) ATP release from intact TDAs in response to adrenergic vasoconstrictors: phenylephrine (PE; 20 μmol/L) and norepinephrine (NE; 20 μmol/L), or non-adrenergic vasoconstrictors: serotonin (5-HT; 40 nmol/L) and endothelin-1 (ET-1; 40 nmol/L). n = 4 mice. Data displayed as groups and represented as mean ± SEM. Two-way ANOVA and Tukey's posthoc test was performed for significance; *$p < 0.05$.

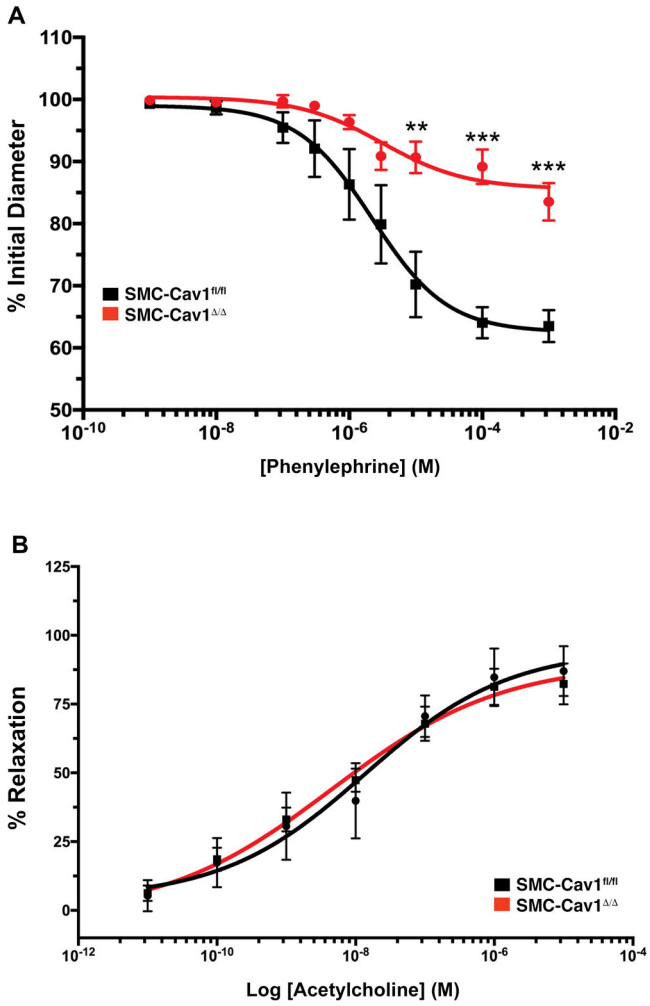

Figure 4. Effects of vascular smooth muscle cell caveolin-1 deletion on vasoconstriction and vasodilation responses in resistance arteries

(A) Contractile responses to increasing concentrations of phenylephrine in TDAs from SMC-Cav1fl/fl control mice (black line; N=4 mice (7 arteries)) and SMC-Cav1Δ/Δ tamoxifen-treated mice (red line; N=6 mice (8 arteries). (B) Effects of VSMC caveolin-1 deletion on endothelial-dependent vasodilation to increasing concentrations of acetylcholine. Concentration-effect curves were fitted to the data using four-parameter, non-linear regression curve. Data assessed by two-way ANOVA with Bonferroni post-hoc test for multiple comparisons. **$p < 0.01$ ***$p < 0.001$.

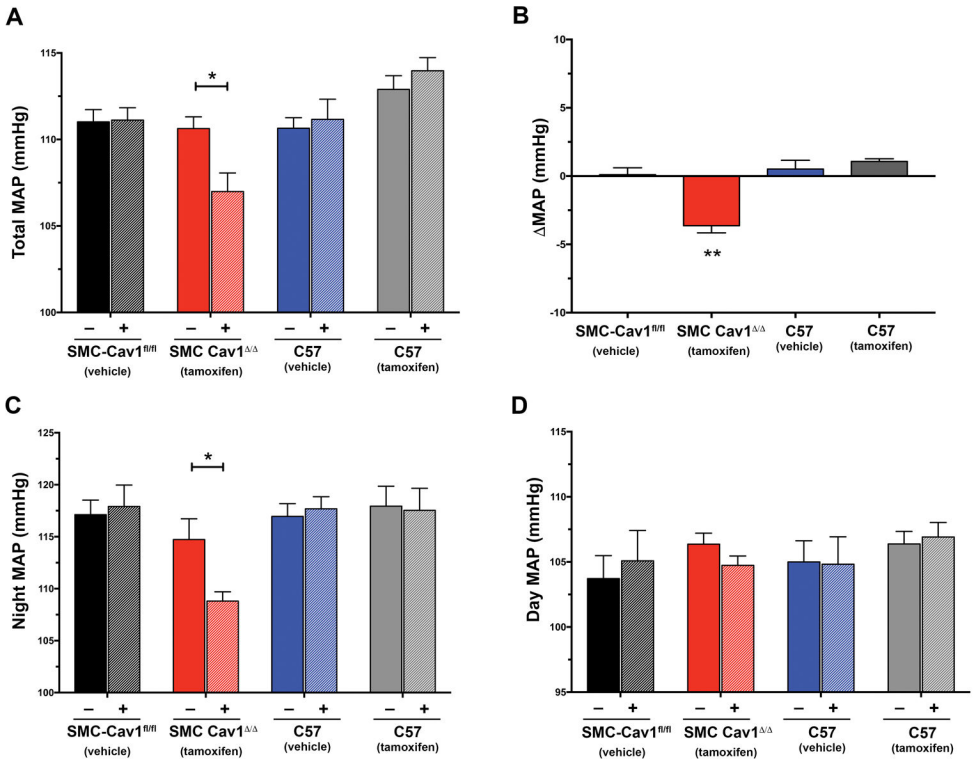

Figure 5. VSMC Caveolin-1 deletion reduces blood pressure

(A) 24 hour mean arterial blood pressure (MAP) of mice across the indicated genotypes. **(B)** Differences in 24 hour MAP (ΔMAP) across the indicated groups of mice after treatment with tamoxifen or vehicle control. **(C)** MAP during the nocturnal active period (12 hr dark: 6:00PM–5:59AM), and **(D)** MAP during the daytime inactive period (12 hr light: 6:00AM–5:59PM). Baseline measurements were made for each individual animal before injections and compared to BP responses 2 weeks after tamoxifen or vehicle control injection. N=4 mice for each treatment group. *$p < 0.05$, **$p < 0.01$, ***$p<0.001$ compared to baseline response using one-way ANOVA (B) or two-way ANOVA (A, C, D), with Tukey's posthoc test.

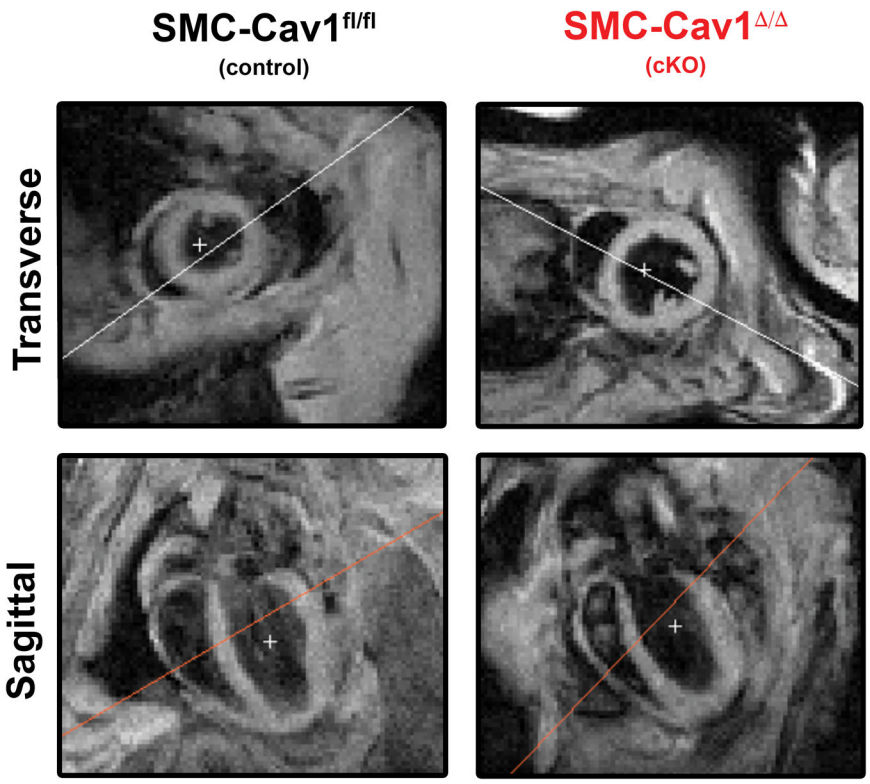

Figure 6. VSMC caveolin-1 deletion does not influence cardiac function

Representative transverse and sagittal MRI images of SMC-Cav1$^{fl/fl}$ control and SMC-Cav1$^{\Delta/\Delta}$ hearts. Six short-axis slices were acquired from base to apex, with slice thickness equal to 1mm, in-plane spatial resolution of 0.2 × 0.2 mm^2, and temporal resolution of 8–12 ms. No differences in size, morphology, or function were detected as summarized in Table 1.

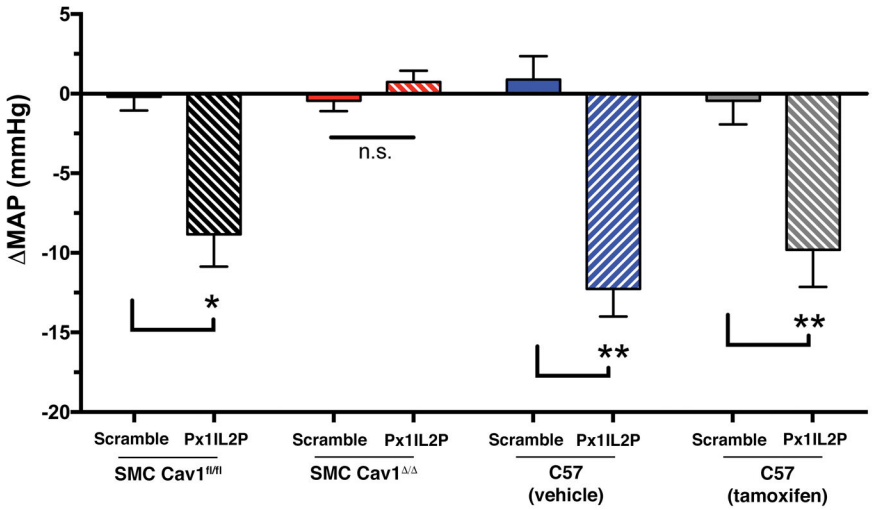

Figure 7. Caveolin-1 deletion prevents the blood pressure-lowering effects of the Panx1 inhibitory peptide (PxIL2P)

Differences in MAP (ΔMAP) measured at baseline and 2 hrs after treatment with the Panx1 inhibitory peptide PxIL2P (20 mg/kg) or scramble control (20 mg/kg) in SMC-Cav1$^{fl/fl}$, SMC-Cav1$^{\Delta/\Delta}$, or C57BL/6 mice. Changes in MAP were calculated using each animal's individual baseline pretreatment. n=4 mice for each treatment group; *p< 0.05 and **p< 0.01 compared to individual baseline response using two-way ANOVA and Tukey's test.

Table 1

Cardiac function is unaltered in VSMC caveolin-1 deficient mice

MRI was performed on a 7 Tesla (T) Clinscan system (Bruker, Ettlingen, Germany) equipped with actively shielded gradients with a full strength of 650 mT/m and a slew rate of 6666 mT/m/ms. Baseline LV structure and function were assessed. Six short-axis slices were acquired from base to apex, with slice thickness equal to 1mm, in-plane spatial resolution of 0.2 × 0.2 mm^2, and temporal resolution of 8–12 ms. Baseline EF, end-diastolic volume (EDV), end-systolic volume (ESV), myocardial mass, wall thickness, and wall thickening were measured from the cine images using the freely available software Segment version 2.0 R5292 (http://segment.heiberg.se). EDV and ESV were then indexed to body mass (EDVI and ESVI, respectively). Mass to volume ratio (MVR) was calculated as the ratio of myocardial mass to EDV. A Student's t-test (two tailed) was performed for significance; * $p<0.05$.

Cardiac function measured by MRI in SMC-$Cav1^{\Delta/\Delta}$ and SMC-$Cav1^{fl/fl}$ control mice. R-R wave ECG interval (R-R), Left Ventricle Mass (LVM), Cardiac output (CO), Ejection Fraction (EV), End Systolic Volume (ESV), End Diastolic Volume (EDV), Stroke Volume (SV). Data represented as mean ±SEM, n=4, 2-tail homoscedastic Student's t-test.

	SMC-$Cav1^{fl/fl}$		SMC-$Cav1^{\Delta/\Delta}$		p-value
Heart Rate [BPM]	489.35	±5.47	491.48	±19.26	0.91
R-R [ms]	122.65	±1.38	122.51	±4.89	0.98
LVM [ml]	0.099	±0.003	0.096	±0.004	0.50
LVM [g]	0.104	±0.003	0.101	±0.004	0.50
EDV [ml]	0.043	±0.003	0.040	±0.004	0.47
ESV [ml]	0.019	±0.002	0.017	±0.002	0.59
SV [ml]	0.025	±0.002	0.022	±0.004	0.59
EF [%]	57.25	±3.05	55.52	±7.29	0.81
CO [l/min]	0.012	±0.001	0.011	±0.002	0.54